The Astrophysical Journal, 669:1262–1278, 2007 November 10

MOLECULAR LINE RADIATIVE TRANSFER IN PROTOPLANETARY DISKS: MONTE CARLO SIMULATIONS VERSUS APPROXIMATE METHODS

Ya. Pavlyuchenkov, D. Semenov, and Th. Henning
Max Planck Institute for Astronomy, Königstuhl 17, D-69117 Heidelberg, Germany

St. Guilloteau
Laboratoire d'Astrophysique de Bordeaux, OASU, Université Bordeaux 1, CNRS, 2 rue de l'Observatoire, BP 89, F-33270 Floirac, France

V. Piétu
IRAM, 300 rue de la Piscine, F-38406 Saint Martin d'Hères, France

R. Launhardt
Max Planck Institute for Astronomy, Königstuhl 17, D-69117 Heidelberg, Germany

and

A. Dutrey
Laboratoire d'Astrophysique de Bordeaux, OASU, Université Bordeaux 1, CNRS, 2 rue de l'Observatoire, BP 89, F-33270 Floirac, France
Received 2007 May 8; accepted 2007 July 24

ABSTRACT

We analyze the line radiative transfer in protoplanetary disks using several approximate methods and a well-tested accelerated Monte Carlo code. A low-mass flaring disk model with uniform as well as stratified molecular abundances is adopted. Radiative transfer in low and high rotational lines of CO, $C^{18}O$, HCO^+, DCO^+, HCN, CS, and H_2CO is simulated. The corresponding excitation temperatures, synthetic spectra, and channel maps are derived and compared to the results of the Monte Carlo calculations. A simple scheme that describes the conditions of the line excitation for a chosen molecular transition is elaborated. We find that the simple LTE approach can safely be applied for the low molecular transitions only, while it significantly overestimates the intensities of the upper lines. In contrast, the full escape probability (FEP) approximation can safely be used for the upper transitions ($J_{up} \gtrsim 3$), but it is not appropriate for the lowest transitions because of the maser effect. In general, the molecular lines in protoplanetary disks are partly subthermally excited and require more sophisticated approximate line radiative transfer methods. We analyze a number of approximate methods, namely, LVG, vertical escape probability (VEP), and vertical one ray (VOR) and discuss their algorithms in detail. In addition, two modifications to the canonical Monte Carlo algorithm that allow a significant speed up of the line radiative transfer modeling in rotating configurations by a factor of 10–50 are described.

Subject headings: astrochemistry — line: formation — line: profiles — planetary systems: protoplanetary disks — radiative transfer — radio lines: stars — stars: formation

1. INTRODUCTION

The study of the formation and evolution of protoplanetary disks is an important topic for our understanding of the formation of extrasolar planets and the planets in our solar system. The gas content of the disk that represents most of its mass and has an imprint of earlier evolutionary history is best studied in molecular lines. Since 1997, a number of rotational transitions from simple molecules like CO, CS, CN, HCN, HCO^+, N_2H^+, H_2CO, and C_2H, and some of their isotopes have been firmly detected in several nearby protoplanetary disks with single-dish telescopes and millimeter interferometers (e.g., Dutrey et al. 1997; Kastner et al. 1997; van Zadelhoff et al. 2001; Aikawa et al. 2003; Qi et al. 2003, 2004; Thi et al. 2004; Guilloteau et al. 2006). The wealth of information about disk physical structure and chemical composition can only be acquired with multimolecule, multiline interferometric observations at (sub-) millimeter wavelengths and at subarcsecond resolution (e.g., Qi et al. 2006; Piétu et al. 2007). In 2005, we started a comprehensive observational program at the IRAM 30 m antenna and the Plateau de Bure interferometer aimed at studying protoplanetary disks with several key molecular tracers of disk temperature, density, kinematics, and ionization degree (Chemistry in Disks [CID] project; for the first results, see Dutrey et al. 2007).

However, in order to extract all the relevant information from molecular lines and the thermal dust continuum, one must cope with the inverse (line) radiative transfer (LRT) problem, which can hardly be solved for complex geometrical configurations. Instead, one solves the direct LRT problem; models with varied parameters are compared to the observational data until the best fit is found by using some iterative minimization technique (e.g., Guilloteau & Dutrey 1998; Dartois et al. 2003). Naturally, this task requires enormous amounts of computing power that severely restricts the choice of applicable computational methods. This implies that often fast but only approximate algorithms can be used. Thus, it is crucial to investigate the applicability of such approximate methods for the LRT modeling of protoplanetary disks.

Various one- and multidimensional exact and approximate LRT methods have been developed for the modeling of stellar atmospheres, stellar winds, interstellar clouds, and star-forming regions (for a good overview see, e.g., Peraiah 2001). Among the simplest LRT concepts are the local thermodynamical equilibrium (LTE) and large velocity gradient (LVG) approaches in which the LRT problem is treated locally (see Sobolev 1960; Mihalas 1978). The LVG method is just one among the subclass of "escape probability" approaches that allow the straightforward calculation of the escape probability. These simplified LRT methods have been applied to constrain the basic physical parameters of dense molecular cores using single-dish molecular line data (see, e.g., de Jong et al. 1975; Guilloteau et al. 1981; Goldsmith et al. 1983).

Later, more sophisticated, nonlocal LRT approaches have been developed, starting from the one-dimensional methods (e.g., Lucas 1974; Elitzur & Asensio Ramos 2006) to the multidimensional (accelerated) Monte Carlo, local linearization, and multizone escape probability methods (e.g., Bernes 1979; Juvela 1997; Dullemond & Turolla 2000; Hogerheijde & van der Tak 2000; Ossenkopf et al. 2001; Rawlings & Yates 2001; Schöier & Olofsson 2001; Keto et al. 2004; Poelman & Spaans 2005; for a recent review, see van Zadelhoff et al. 2002). Being more accurate, modern LRT methods are routinely applied to study the kinematics and chemical structure of prestellar cores in detail (e.g., Pavlyuchenkov et al. 2006; Tafalla et al. 2006), but their use for protoplanetary disks is still the exception (e.g., Semenov et al. 2005; Brinch et al. 2007).

The global appearance of the physical structure of protoplanetary disks is commonly treated in the framework of steady state passive or active flaring disk models with or without an inner rim, which seem to be successful in explaining many observational facts (e.g., D'Alessio et al. 1998, 2001; Dullemond et al. 2001). The modeled structure can further be used to unravel the chemical evolution of the disk with a sophisticated gas-grain chemical model including surface processes and even dynamical mixing and advective motions (e.g., Willacy et al. 1998; Aikawa et al. 2002; Gail 2002; Ilgner et al. 2004; Semenov et al. 2004, 2006; Willacy et al. 2006; Tscharnuter & Gail 2007). Finally, the disk physical structure and chemical composition together with appropriate collision rates provide the necessary inputs for the LRT simulations.

Since the iterative procedure to search for the best fit to the observed spectra can easily become computationally prohibitive when the full LRT must be considered, it is of great importance to identify those fast approximate LRT methods that give sufficiently accurate results (with respect to the observational limitations) and to investigate the limits of their applicability. The analysis is further complicated when a realistic disk chemical structure is taken into account. To the best of our knowledge, a detailed benchmarking of various approximate LRT approaches for protoplanetary disks has not yet been attempted in the literature apart from the work by van Zadelhoff et al. (2001) and therefore constitutes a major goal of the present paper.

In this paper, we compare a full two-dimensional non-LTE Monte Carlo code with several approximate line radiative transfer methods by considering a few representative radiative transfer cases. These problems are thought to cover all possible situations encountered in disks, namely, the excitation of optically thin/thick emission lines in low-/high-density regions. Consequently, we consider low and high transitions of key molecules in disks tracing temperature (CO and isotopologues), column density (^{13}CO or C^{18}O), density (CS and H_2CO), deuterium fractionation (DCO^+), ionization degree (HCO^+), and photochemistry (HCN). For this exploratory study we adopt an irradiated flaring model of a young, low-mass T Tauri protoplanetary disk, and use both uniform molecular abundances and those from an advanced chemical model (§ 2). Our two-dimensional Monte Carlo algorithm is based on the one-dimensional code RATRAN (Hogerheijde & van der Tak 2000) with two acceleration modifications for disks (see § 3). The adopted approximate methods include the classical LTE approach, the full escape probability (FEP) and vertical escape probability (VEP) methods, LVG, and a nonlocal one-dimensional method, the vertical one ray (VOR) method. The approximate methods are all described in § 4. Using the input disk model and the above LRT methods, in § 5 we calculate the corresponding excitation temperatures, synthetic spectra, and channel maps and compare these data to the results obtained with the Monte Carlo code. The discussion and final conclusions follow.

2. DISK PHYSICAL AND CHEMICAL STRUCTURE

We consider a typical protoplanetary disk surrounding a T Tauri–like star in the nearby Taurus-Auriga molecular complex at 140 pc. A flaring steady state model representative of a Class II disk with vertical temperature gradient is adopted (D'Alessio et al. 1999). The disk has inner and outer radii of 0.037 and 800 AU, respectively, a mass of 0.07 $M_\odot$, and a mass accretion rate of 10^{-8} $M_\odot$ yr^{-1}. The central star has a radius of 2.64 $R_\odot$, a mass of 0.7 $M_\odot$, an effective temperature of 4000 K, and an age of about 5 Myr (see Table 2 in Dutrey et al. 2007). We assume that the disk has a constant microturbulent velocity of 0.1 km s^{-1} and a purely Keplerian rotation profile, $V(r) \propto r^{-1/2}$ (Dartois et al. 2003; Piétu et al. 2007). The disk structure is shown in Figure 1, and the parameters are summarized in Table 1.

In the present study we focus on the molecules that have been detected in protoplanetary disks and are readily used as probes of the disk physical and chemical structure, high-energy radiation, and deuterium fractionation: CO, ^{13}CO/C^{18}O, HCO^+, DCO^+, HCN, CS, and H_2CO. Corresponding to the different excitation conditions, the various rotational lines of these molecules are thought to be generated in distinct disk regions ranging from the cold midplane and warm molecular layer to the hot disk surface layer.

Normally, one must use a sophisticated gas-grain chemical network with surface reactions in order to obtain realistic abundance distributions of these observable species in the disk (see van Dishoeck & Blake 1998; Aikawa & Herbst 1999; Markwick et al. 2002; Semenov et al. 2005; Willacy et al. 2006). For many molecules their highest concentrations are reached in the disk intermediate layer (at $\sim$0.5–1 pressure scale heights) that is sufficiently opaque to destructive high-energy radiation and yet too warm for effective freeze-out of gas-phase molecules (e.g., Aikawa et al. 2002; Dutrey et al. 2007). As a result, in these models from a qualitative point of view, the abundance distributions of many molecules can be represented by a single layer with particular concentration, thickness, and location in the disk (see, however, Semenov et al. 2006; Aikawa 2007).

However, for the first simple analysis of the observational data, it is often sufficient to assume that molecular abundances are constant (with respect to hydrogen). Moreover, the use of uniform molecular abundances can help to disentangle most important line radiative transfer effects from strong chemical gradients in the disks.

We adopt both approaches. The values of the uniform molecular concentrations and parameters of the molecular layers are obtained by using the gas-grain chemical model with surface reactions of Semenov et al. (2005). In essence, this model is based on the UMIST 95 database of gas-phase reactions (Millar et al. 1997), a set of surface reactions from Hasegawa et al. (1992) and Hasegawa & Herbst (1993) on 0.1 μm silicate grains, and includes a small deuterium network from Bergin et al. (1999).

The location of each molecular layer in the disk is constrained by the upper and lower boundaries that can be approximated by a power law, $z(r)/H_p(r) \approx a \times r^b$ [where r is the radius in astronomical units and $H_p(r)$ is the pressure scale height as defined in Dartois et al. (2003)]. We assume that the molecular abundances are constant across a molecular layer and use the maximum values in the uniform disk model (Fig. 1). Note that the CS abundances peak toward the inner disk region and cannot be accurately represented by such a simple one-zone model. The parameters of the uniform and layered chemical structures, i.e., parameters $a_{\rm min}$, $b_{\rm min}$ and $a_{\rm max}$,

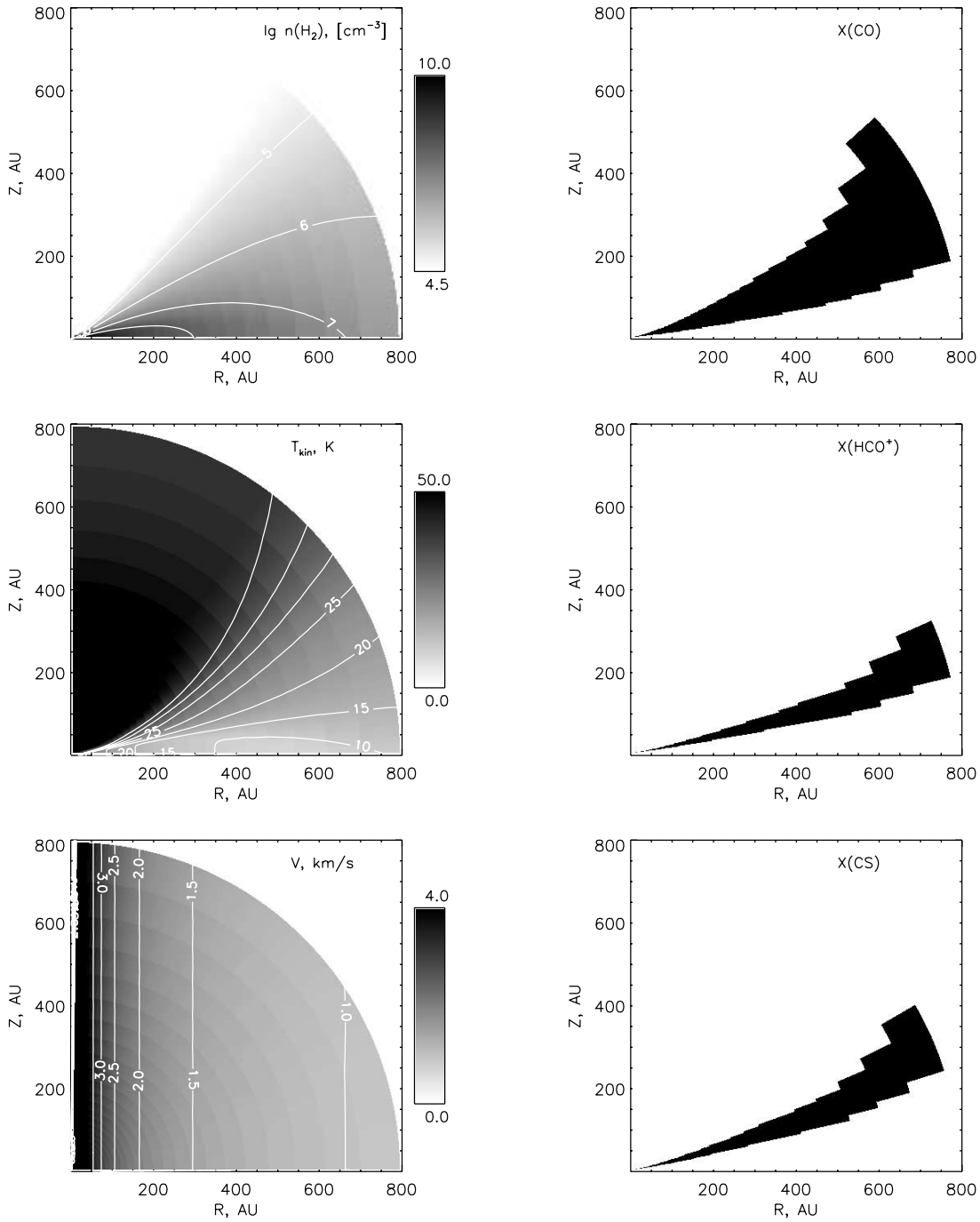

FIG. 1.—*Left*: Distributions of density, temperature, and radial velocity in the adopted disk model. *Right*: Distributions of the molecular abundances relative to the total amount of hydrogen nuclei for CO, HCO^+, and CS.

b_{max} describing the upper and lower boundaries as defined above, are presented in Table 2. Finally, the collision rates for the line radiative transfer modeling are taken from the publicly available Leiden Atomic and Molecular Database[1] (see Schöier et al. 2005).

3. ACCELERATED MONTE CARLO METHOD

In this section we describe our implementation of the accelerated Monte Carlo technique in the two-dimensional non-LTE line radiative transfer code ART, which is part of the software package URAN(IA) aimed at the modeling of various objects with different exact/approximate LRT methods.

3.1. *Basic Algorithm*

The general idea of all Monte Carlo radiative transfer methods is to follow the propagation of randomly ejected photons or photon packages through the medium. These codes are based on a straightforward formalism that is easy to implement numerically and are capable of modeling radiative transfer in various complex multidimensional objects with arbitrarily distributed sources of radiation (e.g., Juvela 1997; Wolf et al. 1999; Pinte et al. 2006; Niccolini & Alcolea 2006). However, in order to lower random

[1] Available online at http://www.strw.leidenuniv.nl/~moldata.

TABLE 1
Adopted Parameters of the Disk and Central Star

Parameter	Symbol	Value
Distance	r_*	140 pc
Stellar temperature	$T_{\rm eff}$	4000 K
Stellar radius	R_*	2.64 $R_\odot$
Stellar mass	M_*	0.7 $M_\odot$
Disk inner radius	$R_{\rm in}$	0.037 AU
Disk outer radius	$R_{\rm out}$	800 AU
Disk mass	$M_{\rm disk}$	0.07 $M_\odot$
Surface density at 1 AU	Σ_1	$\approx$63 g cm^{-2}[a]
Density profile	p	≈ -1[a]

[a] Density structure is the outcome of the disk model.

noise and thus retain reliable accuracy of the results, Monte Carlo simulations typically require enormous amounts of computing time, especially for highly optically thick objects. In certain cases the numerically most demanding part of Monte Carlo codes (ray tracing) can be significantly optimized by special iterative schemes for the acceleration of convergence.

The algorithm of our two-dimensional non-LTE line radiative transfer code ART is fully described in Pavlyuchenkov & Shustov (2004) and only briefly summarized here. In essence, this Monte Carlo code is based on the accelerated scheme originally proposed and implemented in the LRT code RATRAN by Hogerheijde & van der Tak (2000) and in the modified Monte Carlo method of Voronkov (1999). The main equations of the line radiative transfer can be found elsewhere (e.g., van Zadelhoff et al. 2002; Rohlfs & Wilson 2004) and are not repeated here.

First, the computational domain is split into cells. All physical quantities are assumed to be constant within each disk cell i, except for the velocity, which can vary. In the first iteration, initial level populations and a set of photon random directions $\boldsymbol{n}(i)$ through the grid are defined (this is the Monte Carlo part of the calculations). The same set of photon random directions is used in all subsequent iterations for accurate ray tracing, producing a solution free of random noise but with possible undersampling of directions and velocities.

Using these values, the line intensities $I_\nu(i)$ are computed for each disk cell i by explicit direct integration of the radiative transfer equation with the long characteristic method along the predefined set of photon rays $\boldsymbol{n}(i)$, starting with the CMB field at the edge of the disk (or interstellar radiation field, or anisotropic stellar radiation). The integration path is split into subintervals with a step that is smaller than the cell size. Ideally, one would need to define this integration step based on local gradients of the physical conditions in the disk and the optical depth of the line. However, this is not easily achievable in practice, so an empirical value must be used. We adopt a step size of 1/10 of the cell size in our computations.

Next, the resulting mean line intensity $\tilde{J}$ is calculated in each disk cell by spatial averaging of the derived intensities $I_\nu(i)$ over directions $\boldsymbol{n}(i)$ and by averaging over the line profile. The computed mean intensities are used in the next iteration step to refine the level populations by solving the balance equations in all disk cells.

The convergence of the integration procedure for optically thick lines can be substantially accelerated by additional internal subiterations similar to the accelerated lambda iterations (ALI) scheme (Auer & Mihalas 1969). The ALI method employs the fact that the calculated mean line intensity at each particular grid cell can be separated into an internal component generated in the cell itself and an external contribution coming from other grid cells. As a result, additional subiterations are applied to bring into an agreement the internal mean line intensity and the corresponding level populations in every grid cell. When these local subiterations converge, the global iterations over the entire grid are continued until the level populations in each cell do not differ by more than 0.1%. Note that this scheme may not be fully appropriate in cases of particularly thick lines with $\tau \gtrsim 100$ when such a simple convergence criterion fails, e.g., for water lines (van der Tak et al. 2005).

After the final molecular level populations are obtained, the maximum random error associated with the Monte Carlo computations is estimated. For that all iterations are repeated again with another set of preselected random photon rays. We choose the number of random photon paths such that the relative error in the computed level populations is smaller than 1%. Although the code is currently restricted to axially symmetric (two-dimensional) radiative transfer problems in polar coordinates, it can be extended to problems with any number of dimensions and for any coordinate system.

Finally, these resulting level populations are used in the three-dimensional ray-tracing part of the URAN(IA) package to produce synthetic molecular line spectra, channel maps, integrated line intensity maps, velocity maps, etc., with an arbitrary number of velocity channels and for any disk-viewing geometry. Beam convolution can be applied if needed.

The URAN(IA) code was carefully benchmarked against other LRT codes by solving several one- and two-dimensional problems. In the one-dimensional regime, the computed molecular level

TABLE 2
Parameters of the Disk Chemical Model

	Molecular Layer					
	Lower Bound		Upper Bound		N(X)/N(H)	
Molecule	$a_{\rm min}$	$b_{\rm min}$	$a_{\rm max}$	$b_{\rm max}$	Layered Abundance	Uniform Abundance
CO	0.7	0.0	2.0	0.0	8×10^{-5}	1×10^{-4}
$C^{18}O$	0.7	0.0	2.0	0.0	2×10^{-7}	2×10^{-7}
HCO^+	1.37	-0.1	1.68	-0.05	6×10^{-10}	1×10^{-8}
DCO^+	0.0	0.0	0.4	0.0	5×10^{-11}[a]	2×10^{-10}
H_2CO	1.37	-0.1	1.2	0.0	3×10^{-10}	1×10^{-8}
HCN	1.75	-0.16	1.92	-0.07	1×10^{-9}	1×10^{-9}
CS	1.44	-0.07	1.83	-0.03	1×10^{-9}	1×10^{-8}

[a] DCO^+ is located in cold outer disk regions at $r \gtrsim 100$ AU.

populations and excitation temperatures are fully consistent with all tests proposed during the conference on molecular radiative transfer[2] (see van Zadelhoff et al. 2002). Several additional tests of our code were performed in two-dimensional mode, using a few simple problems with analytically predictable solutions. In addition, together with M. Hogerheijde (the developer of the two-dimensional LRT code RATRAN) we successfully compared the results for both codes for Keplerian disks.

3.2. *Further Acceleration of the Monte Carlo Algorithm*

3.2.1. *Concept of Interaction Areas*

The method of long characteristics is one of the most reliable algorithms for calculating the mean intensity and, thus, obtaining an accurate solution to the radiative transfer problem (e.g., Dullemond & Turolla 2000). However, a direct realization of this method is computationally expensive for multidimensional radiative transfer simulations. For example, to compute molecular level populations for a two-dimensional disk model having 150 vertical and 50 radial grid points and 1000 photon packages per cell, one needs $\gtrsim$5 days of computational time on a modern PC (Pentium Xeon 2.4 GHz with 1 GB RAM).

However, for certain cases the computational time needed for the ray-tracing part can be efficiently reduced. To illustrate this for a rotating Keplerian disk with a radial velocity gradient, let us consider a cell at a given radius r. The local line width that strongly depends on the temperature and microturbulent velocity in the cell is typically $\sim$0.1–0.2 km s^{-1}, which is significantly smaller than the total velocity dispersion across the disk, $V_{\rm disp} \gtrsim 10$ km s^{-1}. Therefore, due to the Doppler shift, the photons emitted at a peak frequency in a cell rotating with a given velocity can only be absorbed locally by some of the neighboring cells having similar velocities (the so-called interaction area). An example of such an interaction area is shown in Figure 2, where regions of the Keplerian disk that are radiatively coupled to the cell located at $r \approx 130$ AU (Fig. 2, *white spot*) are shown in black.

We modified the ray-tracing algorithm used in the radiative transfer (RT) solver of URAN(IA) such that the iterative integration of the RT equation is only performed over the radiatively coupled regions of the disk. During the first iteration, the radiatively coupled regions for each cell are identified using the full ray tracing and stored in a file. This information is used during the next iterations to integrate the RT equation over the radiatively coupled regions only. Note that the radiatively coupled region will be different for each line of each of the considered molecules. However, for those molecules for which the local lines widths are dominated by nonthermal motions (e.g., microturbulence) this difference will be small.

This modification preserves the flexibility of the accelerated Monte Carlo approach and allows one to decrease the computation time for protoplanetary disks by about 1 order of magnitude and more, retaining the same high level of accuracy. One may use an analytical prescription instead of the preliminary ray tracing, but such a prescription will be model-dependent and thus cannot be easily generalized. Although our concept of the interaction areas in rotating configurations somewhat resembles the idea of the approximate LVG method (see § 4.3), it leads to an *exact* solution of the LRT problem.

3.2.2. *Concept of Thermalized Cells*

The densities in the disk interior are so high that the low-level populations of many molecules are thermalized. Naturally, the thermalized disk cells can be effectively excluded from the global iteration calculations since the radiative effects do not play a role in populating the levels. We use the following approach to determine whether a disk cell is thermalized or not. First, the level populations in the disk are calculated using the simple LTE and FEP approaches (see § 4). These two approximate methods represent two extreme cases to the solution of the LRT problem. The LTE approach tends to overestimate while the FEP method tends to underestimate the populations of high levels in the case of radiative coupling. The cell is supposed to be thermalized if the relative difference between the corresponding LTE and FEP level populations is smaller than an adopted threshold of 10^{-3} to 10^{-2}. This modification leads to an additional computational acceleration of about 10% for HCO^+ and 30% for CO and CO isotopes.

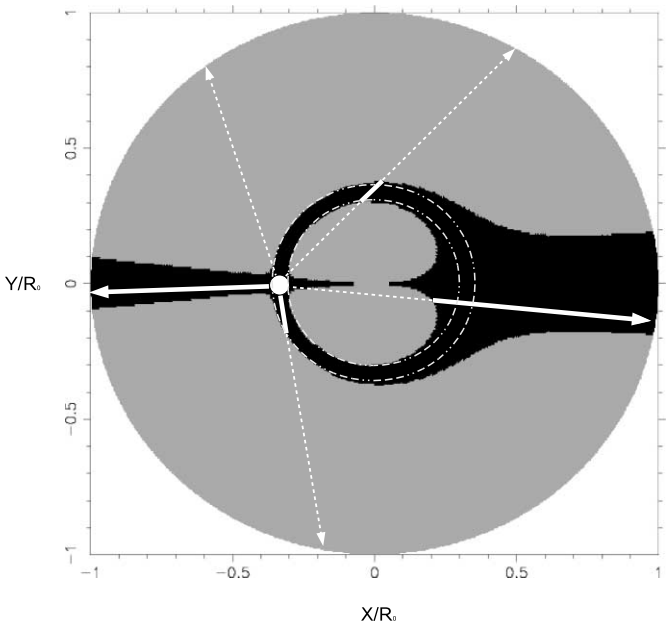

FIG. 2.—Equatorial plane of a Keplerian disk with radius R_0. The white spot represents a rotating cell that emits radiation at a certain rest frequency. The regions where this radiation can be absorbed by the same molecules are shown in black (the so-called interaction area). The interaction area of the disk has velocities that are Doppler shifted from the velocity of the emitting cell by no more than the local line width (expressed in km s^{-1}). The ring bounded by white circles corresponds to the radiatively coupled region in the LVG method.

4. APPROXIMATE LRT METHODS

In this section, we summarize the approximate LRT methods that are compared with the results of the Monte Carlo simulations from the ART code. A schematic overview and comparison of the LRT approaches used is given in Table 3.

4.1. *Local Thermodynamical Equilibrium*

In the case of local thermodynamical equilibrium (LTE), the molecular level populations are thermalized. They follow a Boltzmann distribution with kinetic gas temperature $T_{\rm kin}$,

$$\frac{n_i}{n_j} = \frac{g_i}{g_j} \exp\left(-\frac{h\nu_{ij}}{kT_{\rm kin}}\right), \quad (1)$$

where g_i and g_j are the statistical weights and ν_{ij} is the frequency of the i–j transition. In terms of radiative transfer, thermalization

[2] Available online at http://www.strw.leidenuniv.nl/astrochem/radtrans (G.-J. van Zadelhoff 2002, Leiden Univ.).

TABLE 3
Overview of the Applied LRT Approaches

Method	Type	Applicability	CPU Time[a]
LTE.....	Local	Supercritical region	<1 s
FEP.....	Local	As above and optically thin lines	<1 s
LVG.....	Local	Regions with strong-velocity gradients	~1 s
VEP.....	Local	Regions with low-velocity gradients	~1 s
VOR.....	Nonlocal	Regions with low-velocity gradients	15 m
ART.....	Exact	Everywhere in disks	24 h

[a] CPU times are given for the 128×128 disk grid, 200 photons, and a Pentium 4 2.4 GHz PC.

means that the excitation and kinetic temperatures are equal for a given transition,

$$T_{\rm kin} = T_{\rm exc} = \frac{h\nu_{ij}}{k}\left[\ln\left(\frac{g_i}{g_j}\frac{n_j}{n_i}\right)\right]^{-1}. \quad (2)$$

When the excitation temperature is higher or lower than the kinetic temperature, the level populations are super or subthermally excited.

There are two general situations when LTE holds: (1) the hydrogen density is substantially higher than the critical density of a transition, or (2) the optical depth of a transition is so high that a perfect equilibrium between the collisional and radiative (de-) excitations is reached. The LTE approach is appropriate for the lower rotational transitions of CO and its isotopologues (see Dartois et al. 2003; Piétu et al. 2005). It has also been used in the analysis of molecular line data, even if the conditions for its applicability are not fully justified, because it is the easiest LRT method to implement (e.g., Aikawa et al. 2003; Qi et al. 2003; Narayanan et al. 2006).

4.2. *Full Escape Probability*

Another extreme is to assume that a transition has a very low optical depth, so that the newly generated photons escape the disk freely, without any further interaction with the medium. Or, in other words, in the FEP approach the escape probability β is not calculated and is always set to 1 (see also van der Tak et al. 2007). Under such conditions the LRT problem becomes local and can be easily solved. The FEP level populations are obtained as a solution of the statistical equilibrium equations with the mean intensity J substituted by the mean external radiation field, e.g., CMB: $J = J_{\rm CMB}$. As in the LTE case, the FEP approach requires only very little computational time. FEP can be an adequate method for molecules with very low abundances.

4.3. *Large Velocity Gradients*

In some objects such as expanding stellar envelopes or galaxies, radial velocity gradients can be much larger than the local thermal and microturbulent velocities (e.g., Weiß et al. 2005; Castro-Carrizo et al. 2007). In this case the photons that are emitted by a certain region can only be absorbed locally. The size of this region is determined by the local velocity field and the line width. If one assumes that the physical conditions in this local environment are homogeneous, the radiative transfer problem can be substantially simplified (e.g., Sobolev 1960; Castor 1970; Goldreich & Kwan 1974).

The Keplerian rotation of a circumstellar disk causes strong velocity variations of ~0.5–5 km s^{-1}, which are larger than the local thermal (~0.2 km s^{-1}) and microturbulent (~0.2 km s^{-1}) velocities. As shown in Figure 2, the size of the radiatively coupled zone is significantly smaller than the entire disk plane. Therefore, one may expect the LVG approach to be efficient for the line radiative transfer modeling.

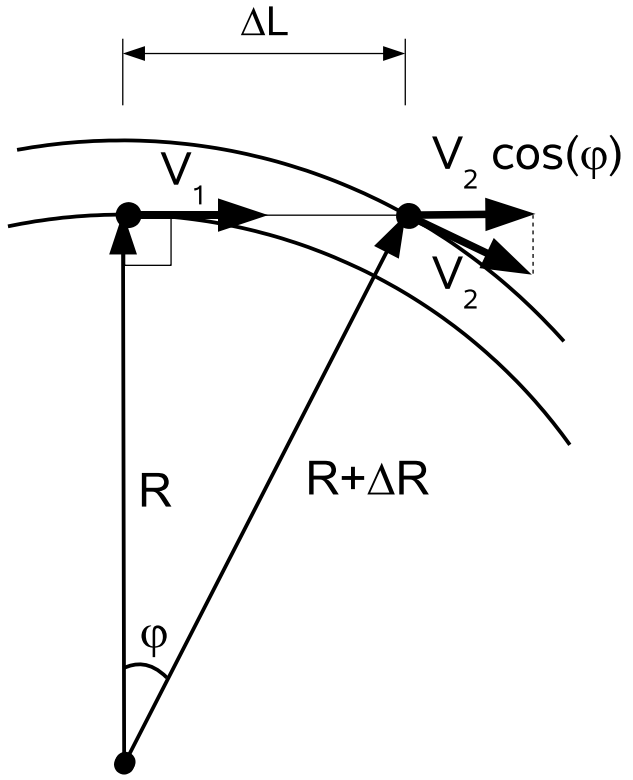

Fig. 3.—Analytical estimation of the coherence length for a rotating disk.

In the LVG method, the mean intensity J in a disk cell is approximated by a combination of the source function S for a given transition and the external radiation field $J_{\rm ext}$,

$$J = (1-\beta)S + \beta J_{\rm ext}, \quad (3)$$

where β is the probability for the photons to freely escape the medium, $0 \le \beta \le 1$. The escape probability β is usually expressed in the form

$$\beta = \frac{1-\exp(-\tau)}{\tau}, \quad (4)$$

where τ is the effective line optical depth because of the local velocity gradient. Note that for optically thin lines the escape probability β reaches unity, and the LVG method turns into the FEP approach.

The effective optical depth τ is evaluated as

$$\tau = \alpha\,\Delta L, \quad (5)$$

where α is the local absorption coefficient and ΔL is the coherence length, i.e., the mean distance for a photon to escape the medium.

The coherence length ΔL in the equatorial plane of the Keplerian disk can be roughly estimated as follows (see Fig. 3). The photons emitted in a disk cell at a radius R cannot escape in the radial direction $\boldsymbol{R}$, since there is no velocity shift in this direction. Instead, we assume that the photons can only escape in the tangential direction. Ideally, one would need to apply spatial averaging to get

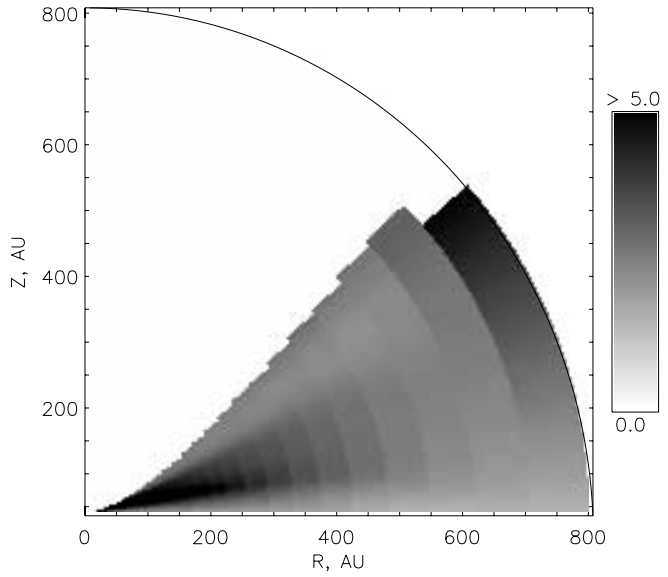

FIG. 4.—Ratio of tangential to vertical optical depths calculated with ART for the uniform disk model and the $HCO^+(4-3)$ line.

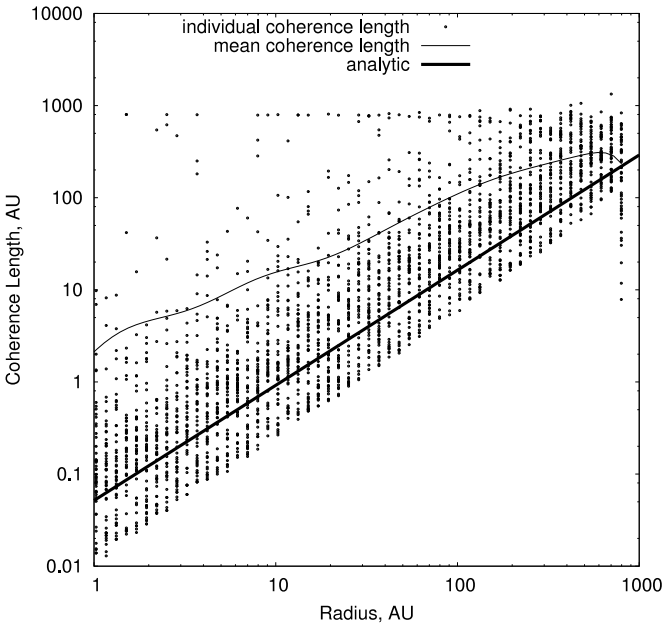

FIG. 5.—Radial dependence of the coherence length (eq. [8]; *thick solid line*) compared to the individual (*circles*) and three-dimensional spatially averaged (*thin solid line*) coherence lengths (ART). The uniform model and the $HCO^+(4-3)$ line are used.

a correct value of the coherence length, but this would significantly complicate the realization of the LVG method.

The approximate coherence length can be expressed via the local line width and the Keplerian velocity. The velocity shift along the coherence path is, by definition, equal to the local line width ΔV,

$$\Delta V = |V_2 \cos(\varphi) - V_1|, \tag{6}$$

where V_1 and V_2 are the Keplerian velocities at the distances of R and $R + \Delta R$, respectively, and φ is the corresponding angle between the velocity vectors (Fig. 3). Expanding the Keplerian velocity into a Taylor series, we find that $V(R + \Delta R) \approx V(R) + \partial V/\partial R \Delta R$, while $\cos(\varphi) \approx R/(R + \Delta R)$. This allows one to derive the value of ΔR from equation (6),

$$\frac{\Delta R}{R} = \frac{2}{3}\frac{\Delta V}{V}. \tag{7}$$

Note that ΔR is the width of the ringlike radiatively coupled region depicted in Figure 2.

From Figure 3 we also find that the coherence length ΔL can be related to the radial shift ΔR and radius R as $\Delta R/\Delta L = \Delta L/R$, and thus

$$\Delta L = R\sqrt{\frac{2}{3}\frac{\Delta V}{V}} \propto R^{5/4} \tag{8}$$

for a constant line width ΔV. This approach is adopted in our LVG method. It typically takes only several seconds of CPU time to calculate the molecular level populations with the LVG approach.

4.4. *Vertical Escape Probability*

One has to keep in mind that in our disk models there is no velocity gradient in the vertical direction and the disk cells are radiatively coupled in the vertical direction, while in the LVG approach, the disk is effectively decoupled in independent parallel planes. Let us compare the coherence length ΔL with the scale height of the disk H_p. For the geometrically thin, isothermal disk $H_p = \sqrt{2}C_s/\Omega$ (for our definition of H_p, see Dartois et al. 2003), where C_s is the sound speed and Ω is the Keplerian angular velocity at radius R. For gray dust opacities the radial temperature profile is $T \propto R^{-1/2}$ (Dullemond 2002) and thus $H_p \propto R^{5/4}$, similar to the scaling of the coherence length. For our disk model $H_p \approx 28$ AU at $R = 100$ AU, while $\Delta L \approx 25$ AU. Therefore, the radiative effects in the vertical and radial directions are comparable over the entire Keplerian disk (at least around the disk midplane) and, by design, the LVG method can only partly account for the radiative coupling.

To better illustrate the role of radiative coupling in the vertical and radial directions, we computed with ART the ratio between tangential and vertical optical depths for the uniform disk model (see Fig. 4). The typical value of this ratio is only about a few over the entire disk, so both directions are important for the line radiative transfer. Using ART, we also calculated the mean coherence lengths in the equatorial plane of the disk. This is done by spatial averaging of individual coherence lengths. The calculated mean and individual coherence lengths are compared to the values from equation (8) in Figure 5. As can be clearly seen, our analytical expression reproduces well the radial dependence of the mean coherence length, but a number of the individual lengths have larger values because of the photon trapping along directions with zero Doppler shifts. As a result, the mean value of the coherence length is typically about 10 times longer than predicted by equation (8).

However, the excitation conditions vary so greatly over the mean coherence length that it cannot be directly put into equations (3) and (4). In order to properly evaluate the total escape probability β, one must average individual escape probabilities rather than the coherence lengths. This requires information about exact physical parameters along all coupled directions, which makes this approach nonlocal and thus far too complicated.

In the LVG approximation the coherence length is determined by the velocity gradients resulting from the Keplerian rotation of the disk. However, as we have shown above the radial radiative coupling is comparable to the coupling in the vertical direction. One can assume that the vertical radiative coupling is more

important than the radial coupling, which leads to significant simplification of the radiative transfer.

This idea is used in the VEP method where photons are assumed to escape only in the vertical direction perpendicular to the disk plane. A simple correction is made to take into account the large asymmetry between the two opposite escape directions; the escape probability is computed by taking the sum of escape probability upward and downward,

$$\beta = \frac{1}{2}\left[\frac{1-\exp(-\tau^-)}{\tau^-} + \frac{1-\exp(-\tau^+)}{\tau^+}\right], \quad (9)$$

where τ^+ is the optical depth toward the disk surface (upward opacity), and τ^- is the optical depth through the disk midplane (downward opacity). The optical depth in upward and downward directions is calculated using the local excitation conditions and the molecular surface densities along the corresponding directions. Note that this assumption is rather coarse in the presence of strong vertical gradients of physical conditions.

Similar to LVG, in the VEP approach the escape probability, source function, and the local optical depth are obtained iteratively. However, the direct implementation of the iterative VEP approach can be dangerous for disk cells with negative excitation temperature. In VEP, these local conditions are extrapolated over the total vertical extent of the disk, and the resulting optical depth can be negative and large. This leads to the physically unrealistic situation that the escape probability can become large, especially during the iterations required to solve the statistical equilibrium equations and the VEP method may fail to converge. To avoid this problem, we control the downward line optical depth τ^- such that it cannot become negative. The upward optical depth is allowed to remain negative, in order to represent weak inversions at the surface layers.

The method was initially developed in the DiskFit software package (see § 4.6). Like FEP, the VEP method takes only a few seconds of CPU time to solve the LRT problem (see Table 3).

4.5. *Nonlocal One-dimensional Method VOR*

In the LTE and FEP methods radiative coupling effects are completely ignored, while in the LVG and VEP approach radiative trapping is only partially treated. Since there is no vertical velocity gradient in the adopted disk model, the cells are generally radiatively coupled in the vertical direction. Furthermore, Figure 2 shows that, with the exception of a relatively narrow cone in the radial direction, a given cell in the disk is only coupled with cells at the same radius, i.e., with regions with the same one-dimensional structure.

Using these ideas, we construct a nonlocal approximate LRT method in which the radiative coupling in only the vertical direction is taken into account (VOR method). This simplifying assumption allows one to use a one-dimensional approach for calculating the mean line intensity J in a disk cell,

$$J = \tfrac{1}{2}(I_1 + I_2), \quad (10)$$

where I_1 and I_2 are the intensities of the radiation coming along the vertical direction from the top and bottom of the disk, respectively. To further accelerate this method, only one central frequency for each emission line is taken into account. This nonlocal RT problem is finally solved using only two photon paths along the vertical direction for the ray tracing. Computational demands of the one-dimensional VOR method are much less than those of the exact two-dimensional code ART. It usually takes about a few minutes of CPU time to obtain the level populations. Note that our VOR approach is another implementation of the Feautrier method (see Feautrier 1964) and resembles the one-dimensional scheme of Lucas (1974).

The one-dimensional methods have been used to represent spheres as well as infinite planes. In the latter case, an Eddington factor of 3 is used to take into account the mean opacity over all possible angles. In our case, since the interaction only occurs in a ring centered around the star, the Eddington factor should be smaller. We have simply used the Eddington factor of 1, like for a sphere.

4.6. *DiskFit*

The described approximate methods are included in the URAN(IA) package. In our study we also used another software package DiskFit. The program DiskFit allows one to model line radiative transfer in disks using various approximate methods as well as to reconstruct basic disk parameters using an advanced χ^2 minimization scheme in the uv-plane (Dutrey et al. 1994; Guilloteau & Dutrey 1998). The program offers three possibilities to solve the coupled equations of statistical equilibrium and RT: LTE, VEP, and a nonlocal one-dimensional approach. The latter is based on the Feautrier scheme (Feautrier 1964) and is an adaptation to the disk geometry of the code developed by Lucas (1974) for the line radiative transfer modeling of interstellar clouds. This one-dimensional method is thus similar to VOR, but uses several frequency points across the line profile. The Eddington factor may also be adjusted if needed.

Once the level populations are derived, the interferometric visibilities as well as beam-convolved channel maps can be computed using the three-dimensional ray-tracing part (Dutrey et al. 1994). Any arbitrary orientations of the disk defined by the inclination and position angles can be used. For that, a three-dimensional regular grid is used, with additional refinement for the central disk region where the surface brightness gradient is very strong. The DiskFit radiative transfer methods and the ray-tracing part were thoroughly compared against those implemented in the URAN(IA) package, and good overall agreement was achieved for the disk level populations and spectral maps for both the optically thin and thick molecular transitions. Therefore, for the rest of the paper, we compare approximate and exact LRT methods from the URAN(IA) package only.

5. RESULTS

Prior to the detailed comparison of various radiative transfer methods described above, we discuss the problem of molecular line formation and excitation conditions in disks in general.

5.1. *Molecular Line Formation in Protoplanetary Disks*

5.1.1. *Excitation Regimes with Uniform Abundances*

Since the thermal and density structure of protoplanetary disks is relatively well understood (e.g., D'Alessio et al. 1998, 2001; Dullemond & Turolla 2000), we can discriminate distinct regimes of line formation.

A particular rotational transition is excited when the molecular hydrogen density exceeds a critical density $n_{\rm cr}$,

$$n_{\rm cr} = \frac{A_{ul}}{\sum_i C_{ui}}, \quad (11)$$

where A_{ul} is the Einstein coefficient and C_{ui} are the collisional rates from the upper level u to all other lower levels i.

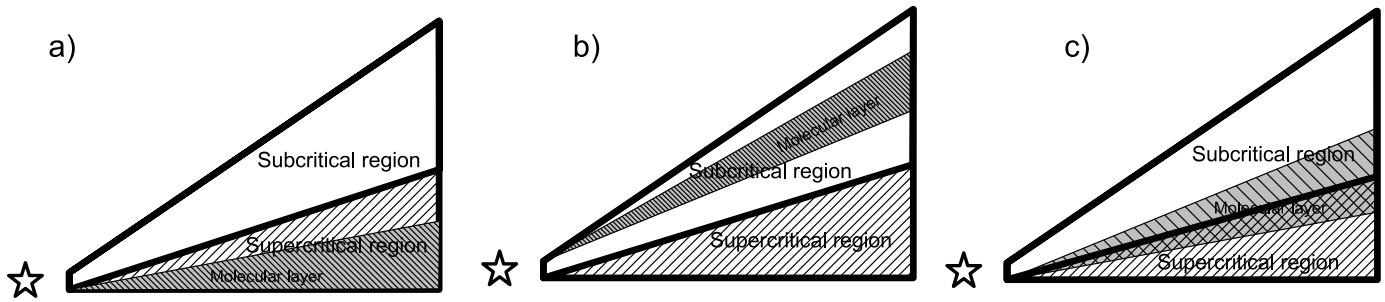

FIG. 6.—Distinct cases of line formation in protoplanetary disks with chemical stratification. *Left*: Molecular layer is located inside the supercritical (high-) density region adjacent to the midplane, and thus, LTE holds for the level populations. *Center*: Molecular layer is located within the subcritical (low-) density region close to the disk surface. The level populations can be accurately calculated either with the FEP method when the molecular column density is sufficiently low or with a more sophisticated nonlocal LRT method (e.g., VOR) when the molecular column density is so high that radiative coupling within the disk becomes important. *Right*: In the most general case the molecular layer lies both in the sub- and supercritical regions. Consequently, FEP is only accurate when the emission mostly comes from the supercritical region of the molecular layer and the optical depth of the subcritical part is low. In all other situations nonlocal line radiative transfer methods must be applied.

The density, $n_{\rm th}$, at which the molecular levels become predominantly populated by collisions and thus are thermalized, is typically about 1 order of magnitude higher than the critical density. We refer to $n_{\rm th}$ as to the thermalization density.

Consequently, the disk can be roughly divided in two regions. In the so-called supercritical region near the disk midplane, where the density is larger than the thermalization density, molecular level populations follow the Boltzmann distribution, and the excitation temperature is equal to the kinetic temperature, $T_{\rm ex} = T_{\rm kin}$. In this region a simple LTE approach can be safely used.

In the upper, more diffuse "subcritical" region of the disk, the line excitation is partly controlled by collisions and partly by internal/external radiation. The crucial parameter that determines the excitation conditions in this region is the molecular column density. If this column density is so high that the subcritical region is opaque to the internal radiation, then the collisional and radiative (de-) excitations are in perfect balance, and the corresponding molecular levels are thermalized, $T_{\rm ex} = T_{\rm kin}$. In contrast, when the column density is so low that the subcritical region is fully transparent to the internal radiation, the corresponding molecular levels are mostly radiatively populated and therefore subthermally excited, $T_{\rm ex} \approx T_{\rm bg}$.[3] In this case a simple FEP approximation can be used (see § 5). The characteristics of the emergent molecular line spectrum will depend on the relative contribution from each of the supercritical and subcritical regions.

5.1.2. *Effects of Chemical Stratification*

This simple scheme becomes more complicated when the effects of chemical stratification are taken into account. In this situation three distinct regimes of line excitation can be distinguished.

In the first and most simple case the molecular layer is located deeply inside the supercritical density region, and the molecular level populations are in LTE (see Fig. 6, *left*). Good examples of that kind are the lower rotational transitions of CO and its isotopologues (Dartois et al. 2003).

In the second case, the molecular layer is entirely confined within the subcritical density region. The distribution of the level populations will then depend on the molecular column density as discussed above (Fig. 6, *center*). When this column density is low and radiative coupling is not important, the FEP approximation works. In the opposite case the radiative transfer problem must be tackled with a more sophisticated nonlocal method. The line excitation proceeds in this way in gas-deficient transition disks (Jonkheid et al. 2006).

Finally, in the most general case the molecular layer is located between the subcritical and supercritical disk regions (Fig. 6, *right*). In this situation the LTE approach does not work, whereas the FEP approximation is valid only if the optical depth of the subcritical layer is low and the molecular emission is dominated by the supercritical (thermalized) layer. The lower rotational lines of, e.g., HCO^+, HCN, and CS are likely excited in such a way.

If the molecular column densities are so large that the subcritical region becomes optically thick for internal radiation, the simple FEP approach fails and nonlocal radiative transfer modeling is required. The non-LTE effects in disks are likely important for the rotational lines of complex species, e.g., H_2CO, but may also be important for higher transitions of many other simple molecules (such as HCN, CS, etc.). In § 5.2 we verify whether non-LTE effects are important in protoplanetary disks and for which molecular transitions this is the case. There we use a simple preliminary analysis of the excitation conditions.

5.2. *Critical Column Density Diagrams*

It is often useful to understand under what conditions a given transition is excited before any LRT modeling is performed. One example is the iterative χ^2 minimization analysis of interferometric data where an approximate LRT method must be used due to limited computational resources (e.g., Guilloteau & Dutrey 1998; Dartois et al. 2003). Usually the basic properties of the physical structure and sometimes the chemical structure of the disks are at least partly known. When the chemical structure is not known, one can use uniform abundance distributions with the abundance values taken from theoretical models.

Using the density and chemical structure of the disk and molecular data as input, one can determine the line optical depth and the amounts of emitting molecules in the sub- and supercritical regions. As discussed in § 4.5, radiative coupling is strong in the vertical direction due to the absence of velocity gradients, and thus, radiative effects on the line excitation are most profound for face-on oriented disks. Plotted as a function of radial distance, the molecular column densities in the sub- and supercritical disk regions as well as the molecular column density needed to reach an optical depth of unity may serve as an indicator of whether and where the considered transition is non-LTE excited and which approximate or exact method is appropriate to model the radiative transfer in this case (see § 5.1).

[3] Here $T_{\rm bg}$ is the temperature of the background radiation, e.g., 2.73 K for the CMB field.

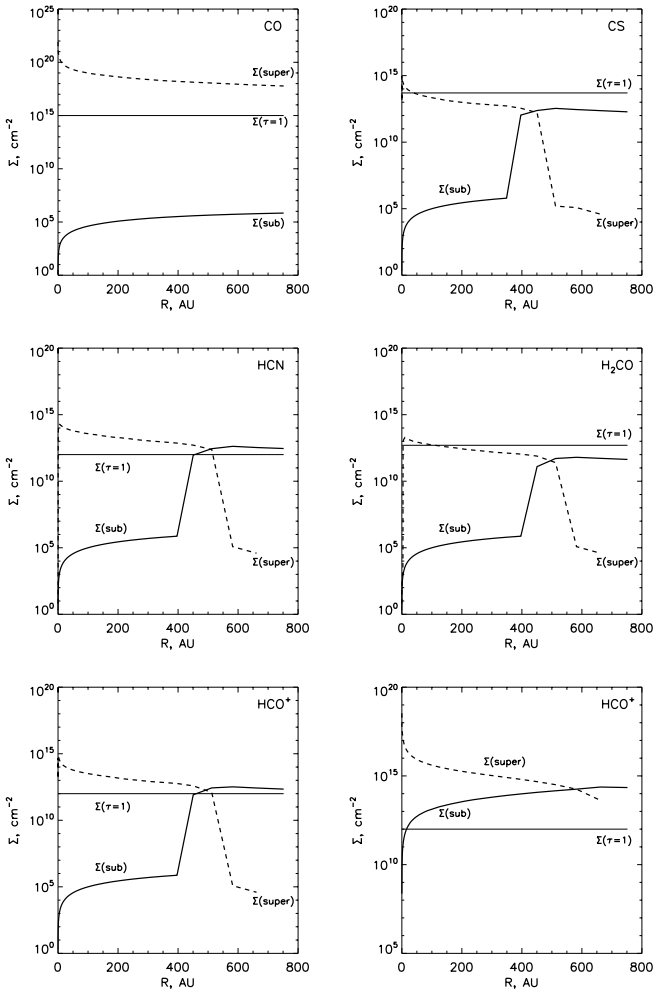

FIG. 7.—Critical column density (CCD) diagrams for (*left to right, top to bottom*) CO, CS, HCN, H_2CO, and HCO^+. For each of these species, the CCD diagram shows the radial distribution of three column densities in the chemically stratified disk: the column density in the subcritical layer (*solid line*), in the supercritical layer (*dashed line*), and the column density that is needed to reach an optical depth of unity for the (1–0) transition (1_{01}–0_{00} for H_2CO; $\tau \sim 1$, *thin solid line*). The uniform HCO^+ model is shown in the bottom right panel. Note that for better presentation the column densities are restricted to values above $\approx 10^6$ cm^{-2}. The ratio between the column densities in the sub- and supercritical layers, together with the value for $\tau = 1$, can be used for preliminary analysis of the line excitation conditions in disks and stimulate the choice of a proper LRT method.

In Figure 7 we present such critical column density (CCD) diagrams for some transitions of the molecules under investigation: CO, CS, HCN, H_2CO, and HCO^+. We focus on low rotational transitions and adopt approximate values of their thermalization densities, viz., 10^5 cm^{-3} for the CO lines and 5×10^6 cm^{-3} for all other molecules. The column densities to attain $\tau = 1$ are computed for the central velocity channel of the (1–0) transition (1_{01}–0_{00} for para-H_2CO), assuming a constant excitation temperature of 10 K.

Not surprisingly, the column density of CO is so high, $N(\mathrm{CO}) \sim 10^{18}$ cm^{-2}, that the lines are very optically thick, $\tau \sim 10^2$–10^3. Since the CO lines are easily excited already at densities of about 10^3 cm^{-3}, essentially all CO molecules are located within the supercritical region (Fig. 6, case a). Molecules tracing the disk interior are excited in similar manner, e.g., H_2D^+, N_2H^+, DCO^+ (Aikawa & Herbst 2001; Semenov et al. 2004; Dutrey et al. 2007). Note that in our model, the CO abundances are high (see Table 2). When comparing with real disks, where CO can be significantly depleted, our test case for $C^{18}O$ can be applied to ^{13}CO observations, while for ^{12}CO, the LTE approximation will work even better (since $\tau = 1$ will be reached at higher densities).

For other less abundant species that have higher critical densities and are concentrated in the disk intermediate layer, the CCD diagrams show a bimodal behavior. In the inner dense disk region at $r \lesssim 400$–600 AU almost all molecules are located in the supercritical region, and their levels are LTE populated (similar to CO). In the outer less dense disk region the molecules are mainly concentrated in the subcritical layer (Fig. 6, case b). The optical thickness of the subcritical region for the disk model with chemical stratification is lower or close to one. Consequently, the molecular subcritical layers are expected to be optically thin or moderately optically thick in the outer disk region, and the FEP approximation holds (see HCN and HCO^+ in Fig. 7). Thus, non-LTE effects should not play a major role for low rotational lines of most molecules in protoplanetary disks. A notable exception is water, which has a complex level structure with a number of maser transitions and some highly optically thick lines (Poelman et al. 2007; van der Tak et al. 2006).

In contrast to the layered chemical structure, for the uniform model the amount of molecules is so high in the subcritical region that this region is optically thick and radiative trapping becomes efficient. As a representative example, we present CCD diagrams for the uniform HCO^+ model (Fig. 7, *bottom right*). In what follows, we focus on this uniform HCO^+ model to analyze in detail the importance of non-LTE excitation for both low and high transitions as modeled by various LRT methods.

5.3. *Excitation Temperatures*

In Figure 8 we show the spatial distributions of the excitation temperature in the uniform disk model as computed by the different LRT methods for the HCO^+ (1–0), (4–3), and (7–6) transitions. By definition, the LTE excitation temperature for any transition is equal to the gas kinetic temperature. The vertical temperature gradient and cold isothermal midplane are clearly visible (Fig. 8, *top*). In contrast, the excitation temperature distributions calculated with other LRT methods show a departure from LTE conditions, in particular, for high transitions and for the upper, less dense disk regions.

The most extreme deviation from LTE is the negative excitation temperature caused by the inversion in the populations of the first two rotational levels of HCO^+ (maser effect), which is reached in the warm upper disk region, at $r \lesssim 200$ AU (white zone in Fig. 8, *left*). In this part the (self-) radiation is not intense, and the levels are excited and de-excited by collisions but only radiatively de-excited. Consequently, LTE is no longer valid, and collisional pumping of the rotational level populations appears as a result of a specific ratio between radiative and collisional (de-) excitation probabilities. Such inversion is characteristic of some linear molecules like CS, HCO^+, and SiO and requires high temperatures and a specific density range (Liszt & Leung 1977; Varshalovich & Khersonskii 1978).

However, this inversion does not result in maser amplification of the HCO^+(1–0) line intensity, even for highly inclined disks. As soon as the line opacity and thus the self-radiation becomes significant, the stimulated radiative transitions depopulate the upper levels and destroy the inversion. Note that in the FEP approximation the effect of self-radiation is completely neglected and therefore the negative excitation temperature zone is strongly overestimated (Fig. 8, *bottom left*).

Another non-LTE zone corresponds to the subthermally excited subcritical disk region, which occupies a significant disk volume for high HCO^+ transitions.

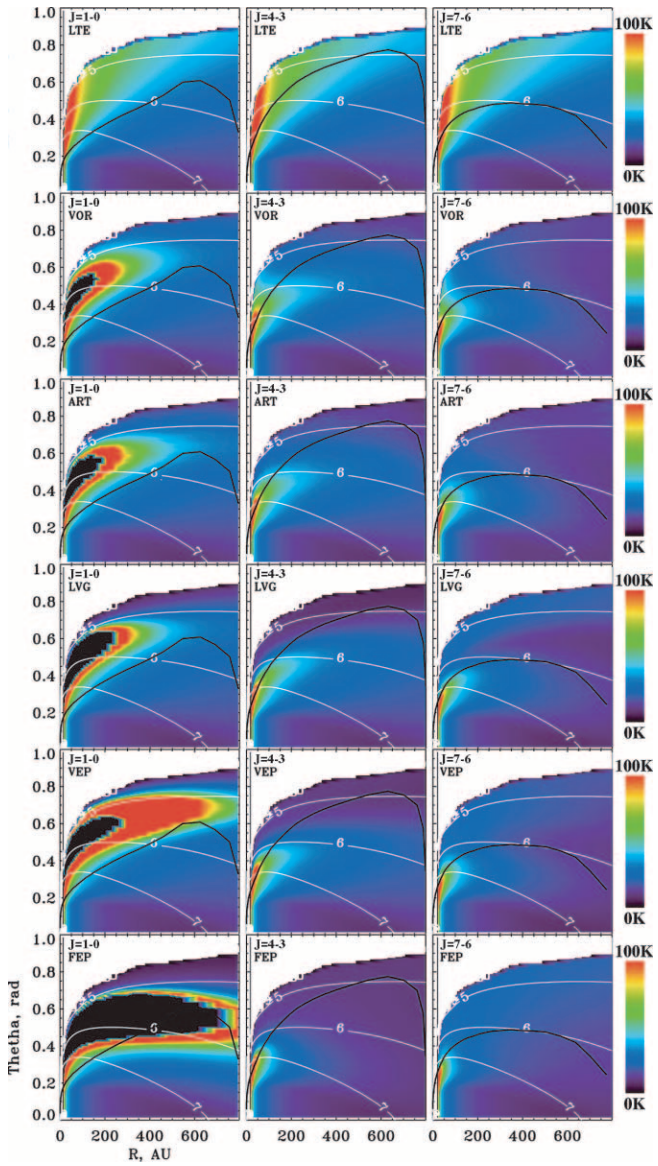

FIG. 8.—Distributions of excitation temperature (*gray scale*, in degrees kelvin) for the HCO^+ $J = (1–0)$, (4–3), and (7–6) transitions (*left to right*) computed with the uniform disk chemical structure (*polar coordinates*). The black line depicts the location of $\tau = 1$ for the corresponding transition, as seen from above the disk in the vertical direction. Vertical scale is angle θ in radians. Shown are the results for the LTE, VOR, ART, LVG, VEP, and FEP radiative transfer methods (*top to bottom*). The white contours correspond to number densities of 10^5, 10^6, and 10^7 cm^{-3}. The white area in the (1–0) distributions marks the zone of negative excitation temperatures (maser effect).

To quantify the difference between the excitation temperature $T_{\rm ex}$ computed with the approximate and exact ART methods, we introduce the local error ϵ in each disk cell,

$$\epsilon = \frac{T_{\rm ex} - T_{\rm ex}^{\rm ART}}{|T_{\rm ex}| + |T_{\rm ex}^{\rm ART}|}. \quad (12)$$

A relative difference of 20% in the excitation temperature corresponds to $\epsilon \simeq 0.1$, and a 35% difference leads to $\epsilon \approx 0.2$.

Consequently, the global accuracy Y of an approximate method over the entire disk can be evaluated with the following expression,

$$Y = \frac{1}{M} \sum_{\tau_j < 1} |\epsilon_j| M_j, \quad (13)$$

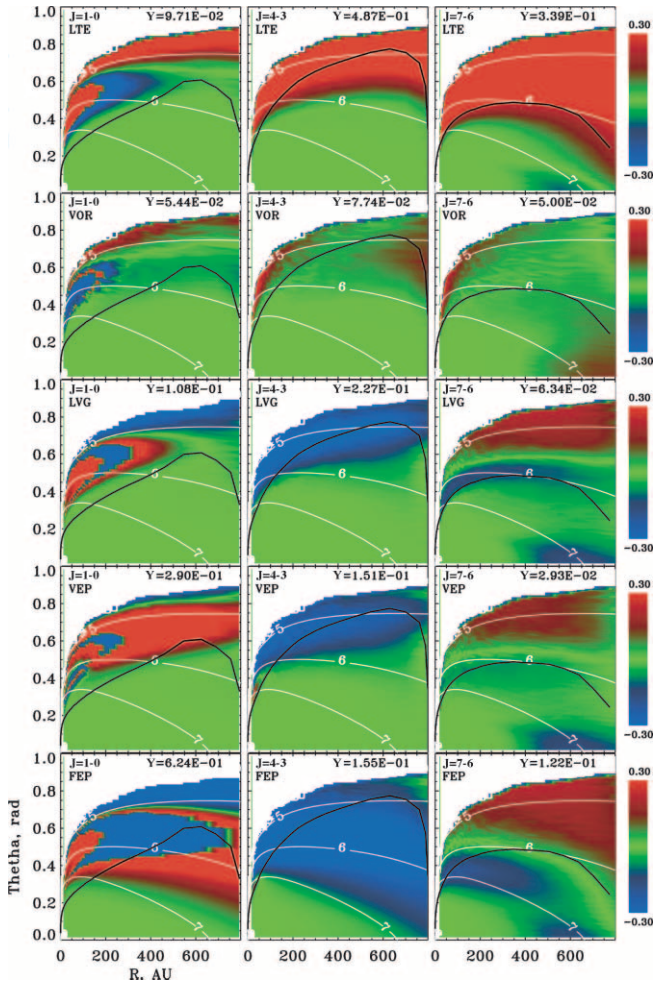

FIG. 9.—Same as Fig. 8, but for the local accuracy estimate ϵ. The thick black line depicts the location of $\tau = 1$ for the corresponding transition, as seen from above the disk in the vertical direction. The accuracy of an approximate LRT method is good when the global error $Y < 0.1$, moderate when $0.1 < Y < 0.2$, and bad when $Y > 0.2$.

where the absolute values of the local errors ϵ_j are summed over the optically thin disk cells and weighted by the number of molecules M_j in each cell. M is the total number of molecules in the optically thin region. The optical depth at the line central frequency, τ_j, is calculated in the vertical direction using the ART level populations.

This global accuracy criterion is designed to directly relate the difference in the excitation temperatures to the difference that will appear in the spectra. We consider disk cells with $\tau \lesssim 1$ (in the vertical direction), because this is the region where most of the line emission comes from (for face-on disks). In essence, the errors in the $\tau \gg 1$ regions are not important, since these regions are not visible. Certainly, this criterion is not a unique one and must be used with care.

We state that an approximate method gives "good" accuracy ("A") if the global criterion $Y < 0.1$, "reasonable" accuracy ("B") when $0.1 < Y < 0.2$, and "bad" accuracy ("C") when $Y > 0.2$. The distributions of the local error ϵ and global accuracy Y of the applied approximate LRT methods for the uniform HCO^+ model are shown in Figure 9.

All LRT methods are accurate in the supercritical disk region, $n \gtrsim 10^7$ cm^{-3}. However, the thermalized disk region extends toward lower densities because the HCO^+ lines are highly optically thick, and the perfect balance between radiative and collisional

TABLE 4
Reliability of the Approximate LRT Methods for the Uniform Model

Molecule	Methods				
	LTE	VOR	LVG	VEP	FEP
CO	AAB	AAA	AAA	AAA	ABB
CS	ACC	AAA	ABA	ABA	BCB
HCO^+	ACC	AAA	BAA	CBA	CCB
HCN	ACC	AAA	ABA	BAA	CCB
H_2CO	ACC	AAA	AAA	AAA	BCA
$C^{18}O$	AAA	AAA	AAA	AAA	AAA
DCO^+	ABC	AAA	AAA	AAA	AAA

Notes.—A: Good accuracy ($Y \leq 0.1$). B: Moderate accuracy ($0.1 < Y \leq 0.2$). C: Bad accuracy ($Y > 0.2$). For all species except H_2CO the first, second, and third letters correspond to the (1–0), (4–3), and (7–6) transition, respectively. For H_2CO the 1_{01}–0_{00}, 4_{04}–3_{03}, and 4_{23}–3_{22} para-transitions are considered.

TABLE 5
Reliability of the Approximate LRT Methods for the Chemical Model

Molecule	Methods				
	LTE	VOR	LVG	VEP	FEP
CO	AAA	AAA	AAA	AAA	AAA
CS	AAC	AAA	AAA	AAA	AAA
HCO^+	ABC	AAA	AAA	AAA	BBA
HCN	ACC	AAA	AAA	AAA	CBA
H_2CO	BBC	AAA	AAA	AAA	AAA
$C^{18}O$	AAA	AAA	AAA	AAA	AAA
DCO^+	AAA	AAA	AAA	AAA	AAA

Notes.—A: Good accuracy ($Y \leq 0.1$). B: Moderate accuracy ($0.1 < Y \leq 0.2$). C: Bad accuracy ($Y > 0.2$). For all species except H_2CO the first, second, and third letters correspond to the (1–0), (4–3), and (7–6) transition, respectively. For H_2CO the 1_{01}–0_{00}, 4_{04}–3_{03}, and 4_{23}–3_{22} para-transitions are considered.

(de-) populations is reached (see § 5.1.1). The thermalized region is particularly large for low rotational transitions that are excited at lower densities.

The LTE approximation tends to significantly overestimate the excitation temperatures for the high transitions with high critical densities but is still appropriate for the $J = (1–0)$ line ($Y \lesssim 0.1$, Fig. 9). In contrast, FEP fails for the (1–0) transition, since it greatly overestimates the region of negative excitation temperature. It is rather accurate ($Y \approx 0.16$) for the (4–3) line, because it adequately describes the excitation conditions in the small, optically thin zone above $\tau = 1$ in the outer disk region, at $r \gtrsim 400$ AU, which occupies the largest volume in the disk. FEP is also accurate for the (7–6) transition ($Y = 0.12$), since it works in the large optically thin region that is decoupled from the internal radiation.

The LVG, VEP, and VOR methods are in general much more accurate than LTE and FEP, because they account for the radiative trapping. In particular, the maser zone in the disk is well reproduced by LVG and VOR. The LVG approach shows the same tendency for the excitation temperature deviations as FEP, because it underestimates the radiative coupling. The nonlocal VOR approach gives the most accurate results for all considered transitions, since it treats the radiative transfer in the vertical direction, where velocity gradients are absent in our model. A minor problem of VOR is the overestimation of the photon trapping in the very upper disk regions where the radiation can escape also in other directions.

In general, for the uniform HCO^+ model and all considered transitions FEP and LTE are not accurate LRT methods ("C" grade), while LVG and VEP are acceptable ("B"), and VOR is good ("A"). This conclusion is valid in general for all other key molecules apart from CO isotopologues where all methods are accurate because their lines arise from the supercritical region (see Table 4). For the disk model with chemical stratification the overall accuracy of all LRT methods is better, because the lines are more optically thin and radiative effects are not that important (Table 5). For many molecular transitions LTE and FEP are reliable approximate methods for the line radiative transfer modeling of chemically stratified disks. However, in this case both LVG and VEP provide an even better approximation, at the expense of very little extra computational time.

5.4. *Synthetic Spectra and Spectral Maps*

Using the excitation temperatures calculated for the uniform chemical structure, we plot the corresponding synthetic HCO^+ spectra for the $J = (1–0)$, (4–3), and (7–6) transitions in Figure 10. All spectra are convolved with the same 10″ beam and are computed for two disk inclinations: $i = 0°$ (face-on) and $i = 60°$.

The LVG, VEP, and VOR methods result in line profiles with intensities deviating by no more than 30% from ART, whereas the FEP and LTE intensities and line profiles differ more strongly from those of ART, in agreement with the difference in excitation temperature maps (see Fig. 9 and Tables 4 and 5). The line intensities computed with FEP and LTE are either overestimated or underestimated, depending on transition. The overall disagreement between these approximate methods and ART does not depend strongly on the disk orientation.

For the HCO^+(1–0) transition the LTE spectrum is close to the ART line profile, but the FEP intensity is 3 times higher for the face-on orientation and even higher for the inclined disk. As discussed in § 5.3, this is due to the maser effect in the first two HCO^+ level populations. The same effect applies to the lower transitions of CS (not shown here). However, for the higher HCO^+ transitions the FEP spectra are in better agreement with the full Monte Carlo simulations, whereas LTE tends to significantly overestimate the line intensities. This is because the size of the radiatively coupled part is decreasing for higher transitions, having higher thermalization densities and thus a more extended subcritical region where $T_{ex} \lesssim T_{kin}$ (compare the top panels in Fig. 9).

At face-on disk orientation a self-absorption dip arises in the (4–3) and (7–6) ART spectra at the central velocity channels. This dip is caused by absorption of emitted radiation in the upper disk region, at $n \lesssim 10^6$ cm^{-3}, due to the vertical excitation temperature gradient (Fig. 8). Both LTE and FEP fail to accurately reproduce this effect. In contrast, the double-peaked HCO^+ spectra of the inclined disk are not due to self-absorption, but appear as a result of the beam convolution over disk cells with different projected velocity. In this case all approximate methods correctly predict the shape of the line profiles. Note that while integrated line intensities do not strongly depend on the disk orientation, the peak intensities do differ strongly and are lower for higher transitions.

The effects of chemical stratification on the integrated spectra are shown in Figure 11. Since HCO^+ occupies only a fraction of the entire disk, the computed line intensities and their optical depths are much lower compared to the uniform model. The self-absorption dip is absent in the face-on line profiles, since there is no more HCO^+ in the upper disk region. The overall agreement between the different LRT methods becomes better (see also Table 5). Still, LTE fails for higher transitions. The detailed comparison for the other species considered here yields similar results.

The criterion Y that gives a global accuracy estimate for the excitation temperature calculated with an approximate LRT method

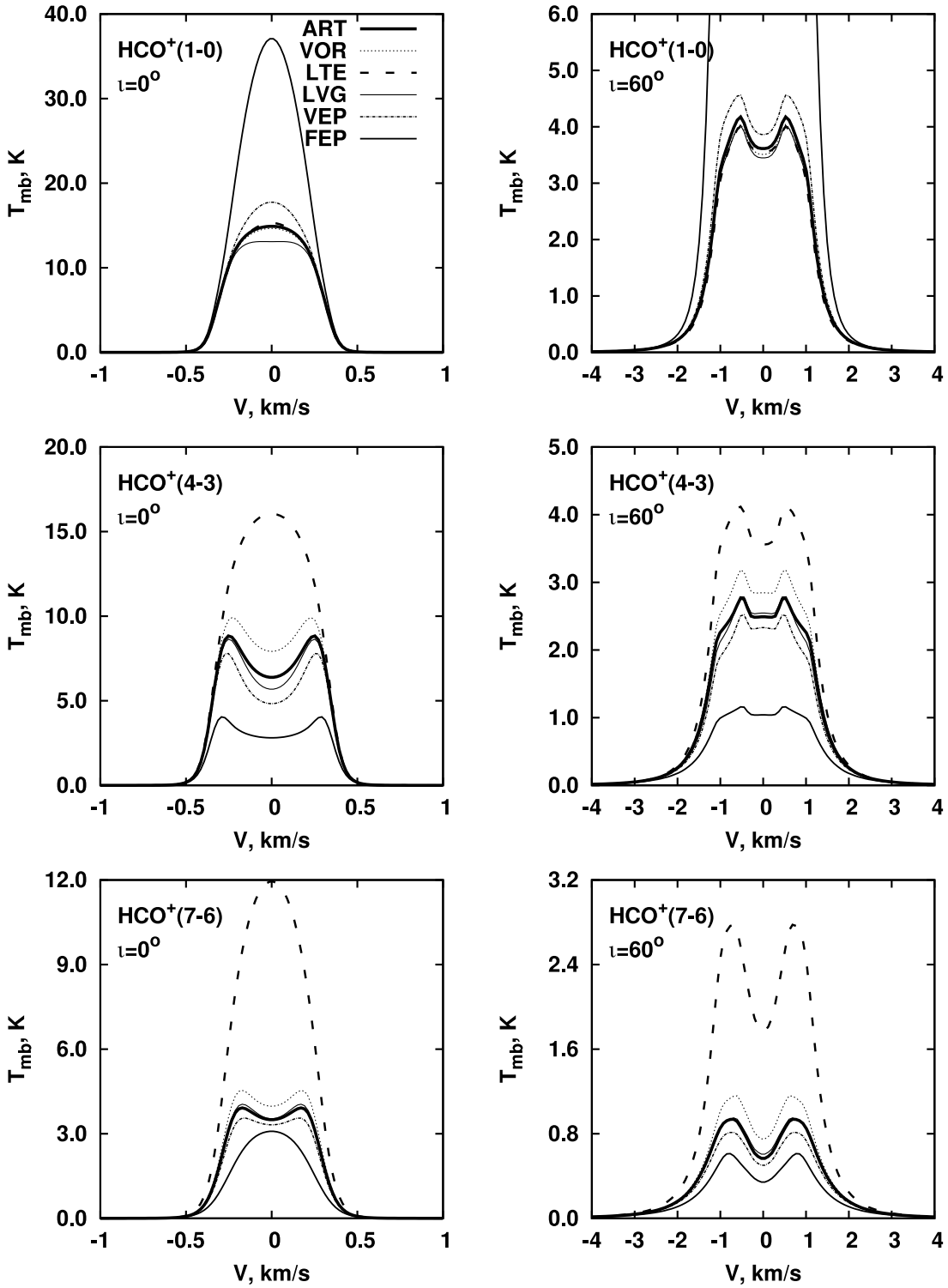

FIG. 10.—Synthetic spectra for the HCO^+(1–0), (4–3), and (7–6) transitions (*top to bottom*) convolved with a 10″ beam. The distance to the disk is 140 pc. The results are obtained with the two-dimensional exact ART (*thick solid line*), the one-dimensional non-LTE VOR (*dotted line*), LTE (*dashed line*), LVG (*thin solid line*), VEP (*dash-dotted line*), and FEP (*medium-weight solid line*) approaches using the disk model with uniform HCO^+ abundances. The disk inclination is 0° (*left*) and 60° (*right*). The intensity is given in units of the main beam temperature (kelvin).

is also valid for the single-dish spectra. To investigate how good this criterion is for the synthetic spectral maps, we plot the HCO^+(4–3) map at the 0.68 km s^{-1} velocity channel for the same 60° inclined disk, but without beam convolution (Fig. 12).

The model with the uniform HCO^+ abundances leads to a fan-like structure with two low-intensity lanes and a high-intensity interior zone (see Fig. 12, *top middle*). The low-intensity lanes correspond to the cold disk midplane with low-excitation temperatures. Similar to the single-dish spectrum (Fig. 10), LTE (FEP) tends to overestimate (underestimate) the total map intensity. The LTE significantly overestimates the excitation temperature in the upper disk region, leading to the formation of two high-intensity

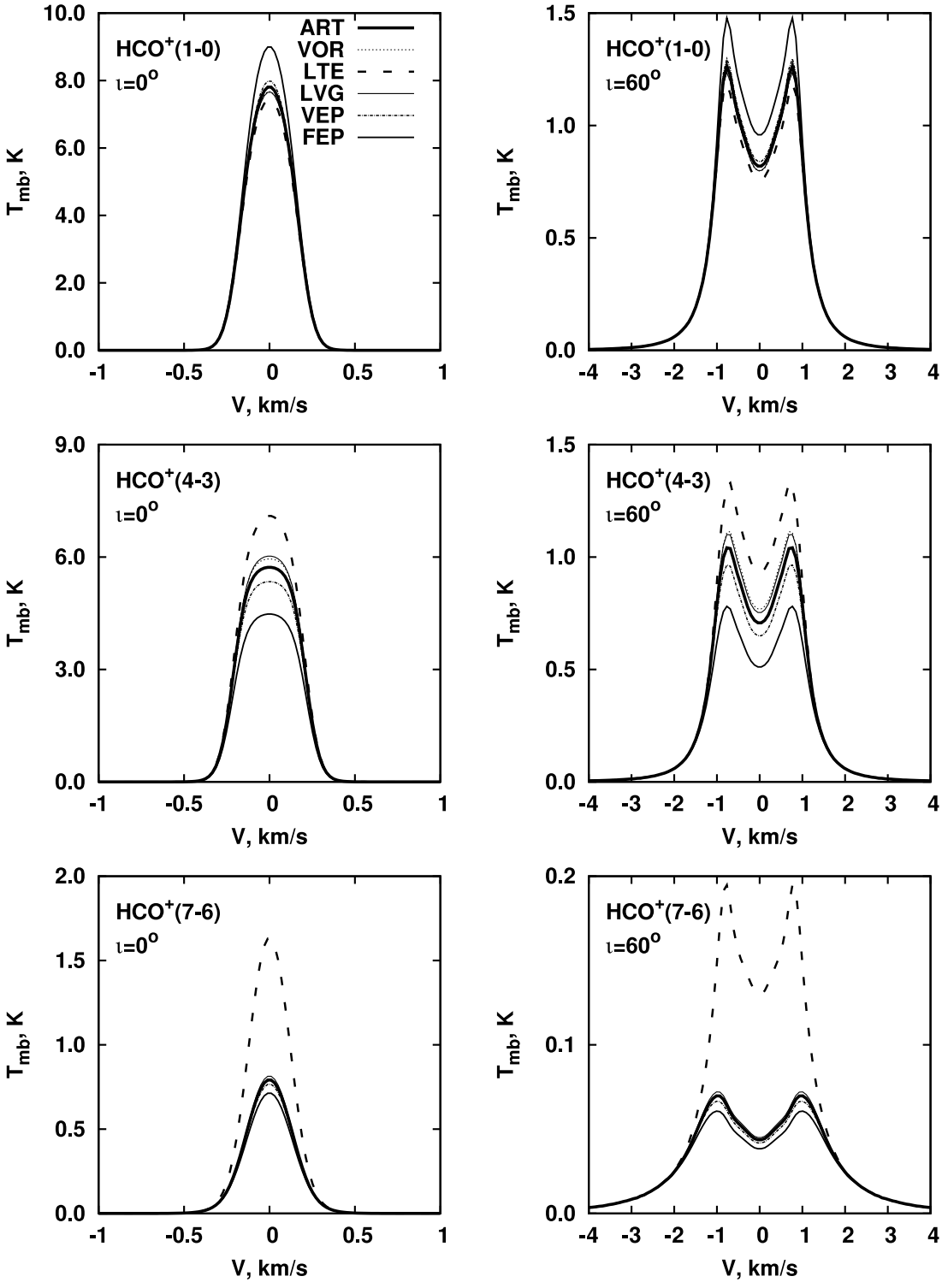

FIG. 11.—Same as Fig. 10, but for the layered HCO^+ abundances from the chemical model.

features near the vertical edges of the image. The contrast of the FEP spectral image is much smaller, yet the cold midplane and high-temperature inner zone are clearly visible in the map.

The LTE, FEP, and ART $HCO^+(4–3)$ maps simulated with the layered chemical structure do not differ so much as for the uniform model (see also Fig. 11). However, the spectral images show a more complicated pattern that resembles two thick elliptical rings overlaid on each other with an angular shift of about 20° and fixed at the center. The three low-intensity lanes correspond to the disk region close to the midplane that is devoid of HCO^+ emission at the chosen velocity channel of 0.68 km s^{-1}. Furthermore, the HCO^+ ions are also absent in the disk upper layer and the overall extension of the map is smaller in the vertical direction compared to the uniform model.

6. DISCUSSION

Our analysis of the line radiative transfer in protoplanetary disks supports and extends the analysis performed by van Zadelhoff

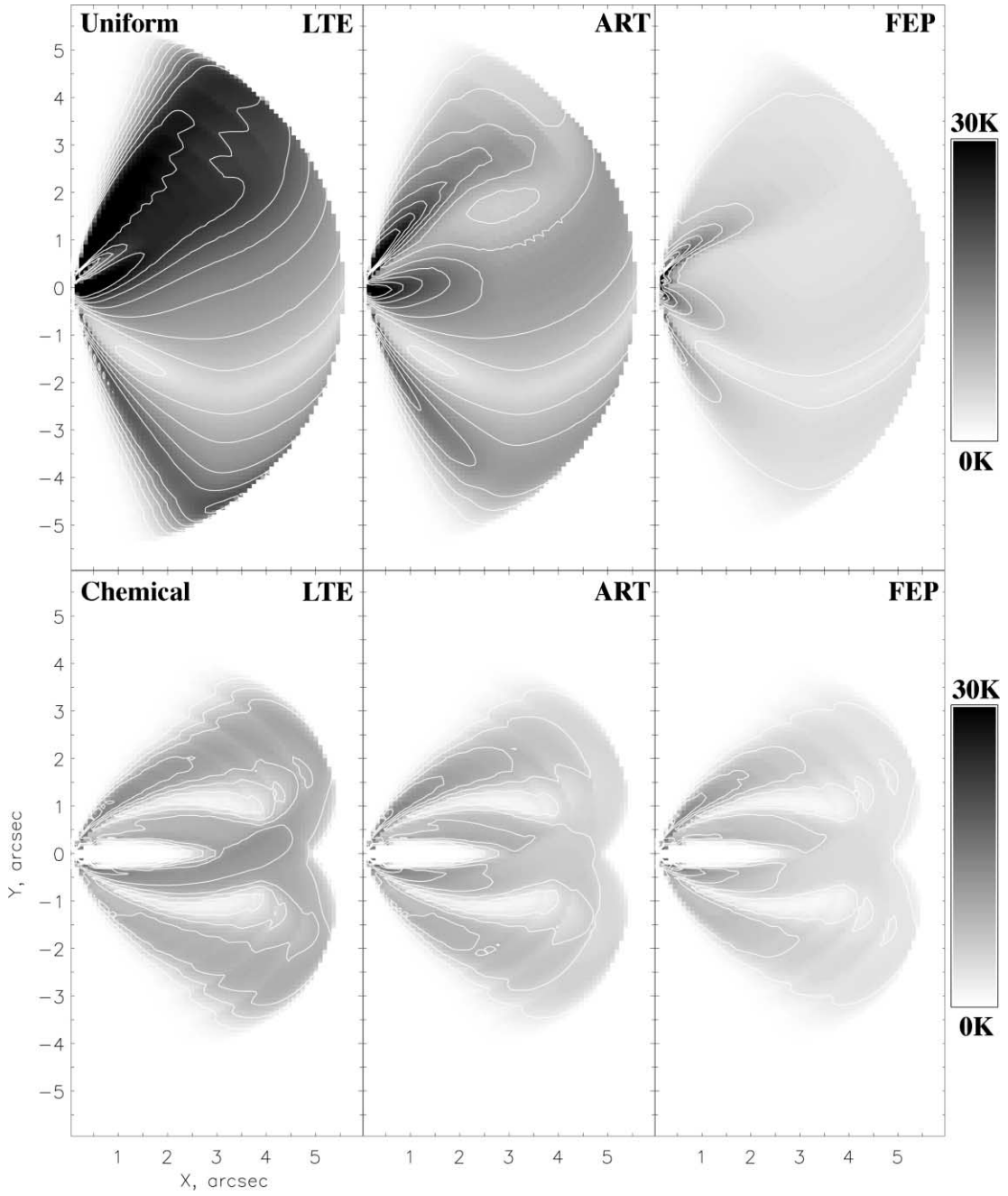

FIG. 12.—HCO^+(4–3) intensity maps synthesized without beam convolution for the 0.68 km s^{-1} velocity channel and for a disk inclination of 60°. The distance is 140 pc. The results are simulated using the level populations computed with the LTE (*left*), ART (*middle*), and FEP (*right*) methods. The uniform (*top*) and layered (*bottom*) abundances of HCO^+ are used. The intensity is given in units of the radiative temperature (degrees kelvin).

et al. (2001). In particular, they argued that SE ($\bar{J}_\nu = 0$) calculations (FEP in our notation) provide better agreement with SE calculations (ART in our notation) compared to LTE. According to our results, the FEP method is indeed more correct than LTE for the upper molecular transitions which were considered by van Zadelhoff et al. (2001). However, the FEP approach may give completely wrong intensities for the lowest molecular transitions such as $J = 1$–0 and $J = 2$–1, since it overestimates the maser effect, resulting from the specific ratio between collisional (de-) excitation rates. Hence, the LTE approach provides more reliable intensities of the lowest transitions than the FEP method. However, LTE fails to reproduce important features of the line profiles like the self-absorption dips. Despite the fact that either LTE or FEP can be sufficient for the simulations of the particular molecular lines, we recommend the use of LVG or VEP, since they provide in general better agreement at the same cost of complexity and CPU requirement. The more exact but more time-consuming methods such as VOR or ART can be used to check the validity of the above approximate methods.

An interesting result of our study is the fact that the synthetic images calculated with VEP are quite close to the exact ART spectra, for both chemically uniform and layered models. This may look surprising, since the idea of the VEP method is to use local

excitation conditions and to extrapolate them along the vertical direction to calculate escape probabilities. Thus, one may expect that this "homogeneous" approach is inappropriate for the disk models with their strong gradients of physical conditions and molecular abundances.

The "good behavior" of VEP is a consequence of the very strong (vertical) density gradient compared to the temperature gradient. In the layered disk model, molecules are concentrated in thin layers where physical conditions do not change much in the vertical direction. In the uniform disk model the strong vertical density gradients result in a supercritical region around the midplane where molecular emission is thermalized, while emission from a low-density surface layer is negligible. In between lies a narrow subcritical disk region, where molecular opacities can be high enough to affect the emergent spectra (see § 5.1). For optically thin lines, the contribution of this narrow layer to the emission is small. For optically thick lines, the likelihood that the line opacity reaches about unity in this region is very low. The exact location of the $\tau = 1$ layer determines the brightness temperature, but is not very critical since vertical temperature gradients are not very large.

Recently, Poelman & Spaans (2005) have proposed a new approximate multizone escape probability (MEP) method to model water line emission from a photodissociation region (Poelman & Spaans 2006). In contrast to our VEP approach, in MEP the probability for photons to escape a cell is computed in three-dimensions by spatial averaging of the optical depths over several (six) directions. Because of its three-dimensional nature, MEP may treat more consistently the photon escape from complicated radiatively coupled regions in Keplerian disks (see Fig. 2) than our VEP method. Since the one-dimensional VEP approach is already reasonably accurate in most cases, the use of three-dimensional MEP for the LRT modeling of protoplanetary disks is recommended in situations when even higher accuracy is required at the expense of extra CPU costs for the spatial averaging.

Another recent one-dimensional escape probability method has been derived by Elitzur & Asensio Ramos (2006). Their coupled escape probability (CEP) approach is based on mathematical transformation of the coupled system of the integro-differential RT equation and linear balance equations into one system of implicit nonlinear equations. Because of fast convergence of this implicit scheme, CEP gains about 1–2 orders of magnitude in computational speed compared to conventional ALI schemes. However, this method cannot be easily adapted to multidimensional LRT problems with multilevel molecules because of the mathematical "trick" that lies behind its algorithm. Taken at face value, in one-dimensional geometry, it would be conceptually similar to, but more sophisticated than, the one-dimensional Feautrier approach implemented in our VOR method.

In the present study we did not consider molecules with complex level structure, e.g., molecules with hyperfine components, since they require more detailed investigations. For instance, Daniel et al. (2006) used new collisional rates to simulate the N_2H^+ lines from prestellar cores and showed that the usual assumption that N_2H^+ sublevel populations follow the Boltzmann distribution may lead to significant errors in the intensities of the hyperfine lines. Van der Tak et al. (2006) mentioned severe problems in LRT simulations of H_2O lines. Apparently, the formation of such complex molecular lines in protoplanetary disks requires a more extended analysis which has to be based on the appropriate collisional rates.

In the present paper, we also did not treat the effects of dust emission on the line formation. For the protoplanetary disks the dust emission at millimeter wavelengths is negligible compared to the molecular transitions. However, at shorter wavelengths the dust emission may be sufficiently strong to excite upper molecular transitions and, therefore, should be considered.

Nor did we include the effects of vertical mixing and turbulence in our model. From a chemical point of view, turbulent diffusion acts as an efficient nonthermal desorption mechanism and smooths molecular abundance gradients in disks (Ilgner et al. 2004; Semenov et al. 2006; Willacy et al. 2006; Tscharnuter & Gail 2007). Consequently, the results for such a disk model would be in between the results for our uniform and layered chemical models.

7. CONCLUSIONS

We analyzed the line radiative transfer and the formation of rotational lines of several key molecules (CO, CS, HCO^+, H_2CO, and HCN) in protoplanetary disks. A detailed model of the disk physical structure with vertical temperature gradient and uniform/layered chemical structure is used. We used the exact accelerated Monte Carlo code ART and compare the results with several approximate LRT approaches, including LTE, the full escape probability (FEP), LVG, and vertical escape probability (VEP) methods and a one-dimensional nonlocal code VOR. Our main conclusions are as follows.

1. Prior to any modeling of the radiative transfer, one can roughly estimate the importance of non-LTE effects for the line excitation and thus choose an appropriate approximate or exact method by using critical column density (CCD) diagrams. The basic idea of the CCD diagrams is to calculate and compare the amount of emitting molecules in the sub- and supercritical regions, taking into account the optical depth of the line. With CCD diagrams we found that the upper disk layers are subthermally excited for many molecular lines, in particular, for the upper transitions.

2. By comparing excitation temperatures, synthesized spectra, and spectral maps, we demonstrate that the simple LTE and FEP methods work reasonably well for chemically stratified disks where molecules are located mainly in the warm intermediate layer or in the disk midplane, but are not always accurate for disk models with uniform abundances. In contrast, the LVG, VEP, and especially, VOR methods take the radiative coupling in the disks into account and thus accurately reproduce the line intensities and profiles. Since the LVG and VEP methods are computationally inexpensive, their use is recommended.

3. We found a possibility for accelerating the ray-tracing part of the RT solver in the Monte Carlo method for rotating disks. In this modification the ray tracing is only performed over radiatively coupled disk zones, leading to a computational speed gain by factors of 10–50.

This work is only the first step in our systematic analysis of the line radiative transfer in protoplanetary disks. The excitation of molecules with complex level structure, including hyperfine line components, and the applicability of various approximate LRT methods for the χ^2 minimization fitting of the observational data will be addressed in future studies.

We thank Michiel Hogerheijde and Jinhua He for useful and stimulating discussions. The authors are thankful to the anonymous referee for valuable comments and suggestions. This research has made use of NASA's Astrophysics Data System.

REFERENCES

Aikawa, Y. 2007, ApJ, 656, L93
Aikawa, Y., & Herbst, E. 1999, A&A, 351, 233
———. 2001, A&A, 371, 1107
Aikawa, Y., Momose, M., Thi, W.-F., van Zadelhoff, G.-J., Qi, C., Blake, G. A., & van Dishoeck, E. F. 2003, PASJ, 55, 11
Aikawa, Y., van Zadelhoff, G. J., van Dishoeck, E. F., & Herbst, E. 2002, A&A, 386, 622
Auer, L. H., & Mihalas, D. 1969, ApJ, 158, 641
Bergin, E. A., Neufeld, D. A., & Melnick, G. J. 1999, ApJ, 510, L145
Bernes, C. 1979, A&A, 73, 67
Brinch, C., Crapsi, A., Hogerheijde, M. R., & Jørgensen, J. K. 2007, A&A, 461, 1037
Castor, J. I. 1970, MNRAS, 149, 111
Castro-Carrizo, A., Quintana-Lacaci, G., Bujarrabal, V., Neri, R., & Alcolea, J. 2007, A&A, 465, 457
D'Alessio, P., Calvet, N., & Hartmann, L. 2001, ApJ, 553, 321
D'Alessio, P., Calvet, N., Hartmann, L., Lizano, S., & Cantó, J. 1999, ApJ, 527, 893
D'Alessio, P., Canto, J., Calvet, N., & Lizano, S. 1998, ApJ, 500, 411
Daniel, F., Cernicharo, J., & Dubernet, M.-L. 2006, ApJ, 648, 461
Dartois, E., Dutrey, A., & Guilloteau, S. 2003, A&A, 399, 773
de Jong, T., Dalgarno, A., & Chu, S.-I. 1975, ApJ, 199, 69
Dullemond, C. P. 2002, A&A, 395, 853
Dullemond, C. P., Dominik, C., & Natta, A. 2001, ApJ, 560, 957
Dullemond, C. P., & Turolla, R. 2000, A&A, 360, 1187
Dutrey, A., Guilloteau, S., & Guelin, M. 1997, A&A, 317, L55
Dutrey, A., Guilloteau, S., & Simon, M. 1994, A&A, 286, 149
Dutrey, A., et al. 2007, A&A, 464, 615
Elitzur, M., & Asensio Ramos, A. 2006, MNRAS, 365, 779
Feautrier, P. 1964, SAO Spec. Rep., 167, 80
Gail, H.-P. 2002, A&A, 390, 253
Goldreich, P., & Kwan, J. 1974, ApJ, 189, 441
Goldsmith, P. F., Young, J. S., & Langer, W. D. 1983, ApJS, 51, 203
Guilloteau, S., & Dutrey, A. 1998, A&A, 339, 467
Guilloteau, S., Lucas, R., & Omont, A. 1981, A&A, 97, 347
Guilloteau, S., Piétu, V., Dutrey, A., & Guélin, M. 2006, A&A, 448, L5
Hasegawa, T. I., & Herbst, E. 1993, MNRAS, 263, 589
Hasegawa, T. I., Herbst, E., & Leung, C. M. 1992, ApJS, 82, 167
Hogerheijde, M. R., & van der Tak, F. F. S. 2000, A&A, 362, 697
Ilgner, M., Henning, Th., Markwick, A. J., & Millar, T. J. 2004, A&A, 415, 643
Jonkheid, B., Kamp, I., Augereau, J.-C., & van Dishoeck, E. F. 2006, A&A, 453, 163
Juvela, M. 1997, A&A, 322, 943
Kastner, J. H., Zuckerman, B., Weintraub, D. A., & Forveille, T. 1997, Science, 277, 67
Keto, E., Rybicki, G. B., Bergin, E. A., & Plume, R. 2004, ApJ, 613, 355
Liszt, H. S., & Leung, C. M. 1977, ApJ, 218, 396
Lucas, R. 1974, A&A, 36, 465
Markwick, A. J., Ilgner, M., Millar, T. J., & Henning, T. 2002, A&A, 385, 632
Mihalas, D. 1978, Stellar Atmospheres (2nd ed.; San Francisco: Freeman)
Millar, T. J., Farquhar, P. R. A., & Willacy, K. 1997, A&AS, 121, 139
Narayanan, D., Kulesa, C. A., Boss, A., & Walker, C. K. 2006, ApJ, 647, 1426
Niccolini, G., & Alcolea, J. 2006, A&A, 456, 1
Ossenkopf, V., Trojan, C., & Stutzki, J. 2001, A&A, 378, 608
Pavlyuchenkov, Ya. N., & Shustov, B. M. 2004, Astron. Rep., 48, 315
Pavlyuchenkov, Ya. N., Wiebe, D., Launhardt, R., & Henning, T. 2006, ApJ, 645, 1212
Peraiah, A. 2001, An Introduction to Radiative Transfer (Cambridge: Cambridge Univ. Press)
Piétu, V., Dutrey, A., & Guilloteau, S. 2007, A&A, 467, 163
Piétu, V., Guilloteau, S., & Dutrey, A. 2005, A&A, 443, 945
Pinte, C., Ménard, F., & Duchêne, G. 2006, in EAS Pub. Ser. 18, Radiative Transfer and Applications to Very Large Telescopes, ed. Ph. Stee (Les Ulis: EDP Sciences), 157
Poelman, D. R., & Spaans, M. 2005, A&A, 440, 559
———. 2006, A&A, 453, 615
Poelman, D. R., Spaans, M., & Tielens, A. G. G. M. 2007, A&A, 464, 1023
Qi, C., Kessler, J. E., Koerner, D. W., Sargent, A. I., & Blake, G. A. 2003, ApJ, 597, 986
Qi, C., Wilner, D. J., Calvet, N., Bourke, T. L., Blake, G. A., Hogerheijde, M. R., Ho, P. T. P., & Bergin, E. 2006, ApJ, 636, L157
Qi, C., et al. 2004, ApJ, 616, L11
Rawlings, J. M. C., & Yates, J. A. 2001, MNRAS, 326, 1423
Rohlfs, K., & Wilson, T. L., eds. 2004, Tools of Radio Astronomy (4th ed.; Berlin: Springer)
Schöier, F. L., & Olofsson, H. 2001, A&A, 368, 969
Schöier, F. L., van der Tak, F. F. S., van Dishoeck, E. F., & Black, J. H. 2005, A&A, 432, 369
Semenov, D., Pavlyuchenkov, Y., Schreyer, K., Henning, T., Dullemond, C., & Bacmann, A. 2005, ApJ, 621, 853
Semenov, D., Wiebe, D., & Henning, T. 2004, A&A, 417, 93
———. 2006, ApJ, 647, L57
Sobolev, V. V. 1960, Moving Envelopes of Stars (Cambridge: Harvard Univ. Press)
Tafalla, M., Santiago-García, J., Myers, P. C., Caselli, P., Walmsley, C. M., & Crapsi, A. 2006, A&A, 455, 577
Thi, W.-F., van Zadelhoff, G.-J., & van Dishoeck, E. F. 2004, A&A, 425, 955
Tscharnuter, W. M., & Gail, H.-P. 2007, A&A, 463, 369
van der Tak, F. F. S., Black, J. H., Schöier, F. L., Jansen, D. J., & van Dishoeck, E. F. 2007, A&A, 468, 627
van der Tak, F. F. S., Neufeld, D., Yates, J., Hogerheijde, M., Bergin, E., Schöier, F., & Doty, S. 2005, in Proc. of the Dusty and Molecular Universe, ed. A. Wilson (Noordwijk: ESA Pub.), 431
van der Tak, F. F. S., Walmsley, C. M., Herpin, F., & Ceccarelli, C. 2006, A&A, 447, 1011
van Dishoeck, E. F., & Blake, G. A. 1998, ARA&A, 36, 317
van Zadelhoff, G.-J., van Dishoeck, E. F., Thi, W.-F., & Blake, G. A. 2001, A&A, 377, 566
van Zadelhoff, G.-J., et al. 2002, A&A, 395, 373
Varshalovich, D. A., & Khersonskii, V. K. 1978, Astron. Zh., 55, 328
Voronkov, M. A. 1999, Astron. Lett., 25, 149
Weiß, A., Walter, F., & Scoville, N. Z. 2005, A&A, 438, 533
Willacy, K., Klahr, H. H., Millar, T. J., & Henning, T. 1998, A&A, 338, 995
Willacy, K., Langer, W., Allen, M., & Bryden, G. 2006, ApJ, 644, 1202
Wolf, S., Henning, T., & Stecklum, B. 1999, A&A, 349, 839